IEEE Journal of Translational Engineering in Health and Medicine

Received 19 January 2023; revised 12 April 2023; accepted 8 May 2023.
Date of publication 10 May 2023; date of current version 24 May 2023.

Digital Object Identifier 10.1109/JTEHM.2023.3275103

An Engineering Platform for Clinical Application of Optogenetic Therapy in Retinal Degenerative Diseases

BOYUAN YAN AND SHEILA NIRENBERG

Department of Physiology and Biophysics, Weill Cornell Medicine, Cornell University, New York, NY 10065, USA
Bionic Sight Inc., New York, NY 10065, USA

CORRESPONDING AUTHOR: S. NIRENBERG (shn2010@med.cornell.edu)

This work was supported by Bionic Sight Inc.

ABSTRACT Optogenetics is a new approach for controlling neural circuits with numerous applications in both basic and clinical science. In retinal degenerative diseases, the photoreceptors die, but inner retinal cells remain largely intact. By expressing light sensitive proteins in the remaining cells, optogenetics has the potential to offer a novel approach to restoring vision. In the past several years, optogenetics has advanced into an early clinical stage, and promising results have been reported. At the current stage, there is an urgent need to develop hardware and software for clinical training, testing, and rehabilitation in optogenetic therapy, which is beyond the capability of existing ophthalmic equipment. In this paper, we present an engineering platform consisting of hardware and software utilities, which allow clinicians to interactively work with patients to explore and assess their vision in optogenetic treatment, providing the basis for prosthetic design, customization, and prescription. This approach is also applicable to other therapies that utilize light activation of neurons, such as photoswitches.

INDEX TERMS Clinical application, neuroprosthesis, optogenetic gene therapy, photoswitches, retinal degenerative diseases.

Clinical and Translational Impact Statement—The engineering platform allows clinicians to conduct training, testing, and rehabilitation in optogenetic gene therapy for retinal degenerative diseases, providing the basis for prosthetic design, customization, and prescription.

I. INTRODUCTION

Optogenetics is a biological technique to control neural activity by expressing light sensitive proteins in neurons [1], [2], [3], [4], [5]. In retinal degenerative diseases, the photoreceptors die, but inner retinal cells remain largely intact. By expressing light sensitive proteins in the remaining cells, optogenetics has the potential to offer a novel approach to restoring vision [6], [7], [8], [9], [10], [11], [12], [13], [14], which is cheaper, less invasive, and more effective than techniques based on retinal implants. Currently, optogenetics has advanced into an early clinical stage [15], [16], [17], [18], and ongoing clinical studies have shown positive results [19], [20], [21].

Despite of the rapid advancement, the development of tools and utilities for clinical applications are lagging. Optogenetic therapy is a particular form of gene therapy in which photosensitivity is conferred to the remaining retinal cells, which typically requires bright light at specific wavelengths for effective activation. In addition, the spatial and temporal patterns of stimulating light also have an impact on the restored vision, which should reflect the visual processing of bypassed retinal pathway. To maximally utilize the optogenetically-restored vision, it is highly desirable to have an engineering platform so that researchers and clinicians can assess and explore the vision of subjects in a systematic and efficient way. The results can be used to measure the outcome of clinical studies as well as provide guidance for the design, customization, and prescription of prosthetic devices.

Similar to prosthetic devices, the key components of such a platform should consist of a stimulating device, capable of delivering bright light at specific wavelengths, with sufficient spatial (e.g., tens of micrometers) and temporal

IEEE Journal of Translational Engineering in Health and Medicine

(e.g., milliseconds) resolution, to cover a large enough visual field, and a software running on a computer, which converts visual stimuli into patterns for light modulation. The conversion from visual stimuli to optogenetic stimulation is often implemented to reflect the neuronal responses to these stimuli in a normal retina [10]. On the other hand, compared to prosthetic devices for individual use, a platform for clinical testing should offer more flexibility and adjustability to allow room for exploration and improvement (e.g., researchers and clinicians could make online changes to many parameters and get immediate feedback from subjects to find the combinations that help the subject see best).

To achieve this goal, we develop a hardware and software platform for clinical training, testing, and rehabilitation. Generally, the platform is applicable to treatments involving light activation of inner retinal cells (such as ganglion cells and bipolar cells), which includes not only optogenetic approaches but also pharmacological approaches, such as photoswitches. In the latter case, chemically synthesized photosensitive molecules (i.e., photoswitches) are employed for manipulating the activation of inner retinal cells (as reviewed in [22]). The system can generate a variety of visual stimuli with adjustable features (size, orientation, moving direction and speed, etc) as well as get live feed from camera to assess different aspects of vision such as light sensitivity, visual acuity, motion and direction, and object recognition. To generate neuronal responses to these stimuli, it is important to find the receptive field of the inner retinal cell, which is nontrivial due to the inhomogeneous architecture in the central retina: there is a radial displacement between inner retinal cells and the corresponding photoreceptors [23]. To address this challenge, the software provides adjustability to account for the displacement in a systematic way.

In addition, the system is capable of performing real-time neural computations with sufficient scalability to meet the requirements for optogenetic retinal stimulation. To target inner retinal cells, optogenetic genes are typically delivered with a single intravitreal injection of adeno-associated virus vectors, and the expression of transgene is often limited to the central para-foveal ring of retina according to studies using non-human primates, as reviewed in [24]. In order to cover this area with cellular resolution, simulation needs to be performed in real-time on a large number of model cells, which poses a challenge on computing power.

Last but not least, it is important to ensure the safety of light exposure. Light safety has been a concern for clinical applications of optogenetics, as early channelrhodopsins required bright light of relatively short wavelengths [1]. The safety margin has been improved with the development of newer optogenetic proteins owing to better light sensitivity and longer peak wavelength [25]. However, extra caution should be taken as recently results showed retinal damage occurred from exposures to 568nm light [26], [27]. The experimental results led to the introduction of a new luminance dose restriction in the 2014 ANSI [28], which significantly lowers the safety margin for longer wavelength. To address this concern, we implement an online safety monitor to keep track of light exposure, which will stop the system once a preset threshold is reached.

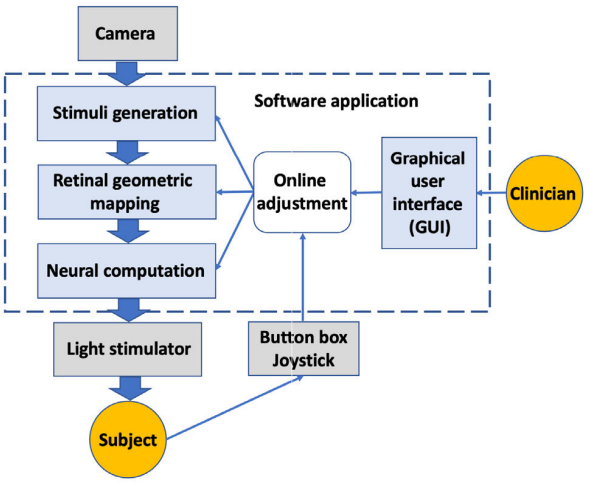

FIGURE 1. Functional diagram. The design consists of a light stimulator and a computer system. A software application is developed to generate a variety of stimuli, which are converted to patterns for light modulation in real time to mimic the function of retinal processing (via retinal geometric mapping and neural computation). The application allows parameters for various functional modules to be adjusted online for clinicians and subjects.

The paper is organized as follows: In Section II, we give an overview of the system. Methods and procedures are presented in Section III, including stimuli generation, retinal geometrical mapping, neural computation, real-time processing, and light safety monitoring. Examples are provided in Section IV to demonstrate the functionality of the system, and a discussion is given in Section V to provide a translational perspective.

II. OVERVIEW OF PLATFORM

In this section, we give an overview of the design, consisting of a light stimulator, which delivers light into the eyes of subjects to activate optogenetic proteins, and a computer system, which drives the light stimulator to perform clinical training, testing, and rehabilitation. A functional diagram is shown in Fig. 1.

A. LIGHT STIMULATOR

For the purpose of visual restoration, it is desirable to deliver light bright enough to effectively activate optogenetic proteins with cellular resolution and millisecond time scale, which is beyond the capability of standard devices such as LCD monitors. To meet these requirements, the light stimulator is built upon a digital light processing (DLP) projector (DLP LightCrafter, Texas Instruments), which is a compact evaluation module for integrating projected light into industrial, medical, and scientific applications. The key component of the module is a digital micromirror device (DMD) [29], a 0.3-inch WVGA chip (DLP3000, Texas

Instruments), consisting of a 608 × 684 array of micromirrors, each 7.6μm × 7.6μm.

In a monochrome pattern mode, the DLP can deliver 24 binary light patterns per frame period. Therefore, the temporal resolution is dependent on the input frame rate. For example, given an input frame rate 60Hz, the output pattern rate is 1440Hz (temporal resolution: 0.7 msec); given an input frame rate 30Hz, the output pattern rate is 720Hz (temporal resolution: 1.4 msec); given an input frame rate 15Hz, the output pattern rate is 360Hz (temporal resolution: 2.8 msec). The system allows to choose one of the three LEDs (blue: 460nm, green: 515nm, red: 617nm).

B. COMPUTER SYSTEM

The light stimulator is driven by a computer system to perform clinical testing, training, and rehabilitation for optogenetic gene therapy. The whole system consists of a computer, a camera, a button box, and a joystick. A software application is developed, capable of generating a variety of visual stimuli, converting stimuli to patterns for light modulation in real time to mimic the function of retinal processing, driving the stimulator to deliver spatially and temporally structured light pulses accordingly, and providing user interface for both offline configuration and online adjustment.

There are two modes in the software application: a training mode and a testing mode. In the training mode, the vision of a subject can be explored interactively to find the optimal parameters for light stimulation, so that vision restoration can be maximized. The training mode offers online adjustability to both researchers/clinicians (with a graphic user interface) and subjects (with a joystick). In the testing mode, the application can be used to conduct testing in blocks of trials with selected visual stimuli, the subject responds by pressing a button on a button box or key on a keypad, and the results are saved on the computer.

In the application, the DMD pixel array is divided into non-overlapping adjacent groups of pixels. The on/off state of the mirrors in each group is controlled by a model cell, one designed to mimic the processing of normal retinal cells (e.g., at the bipolar or ganglion cell level). Given a model cell, the inputs are specified by a set of pixels within the cell's receptive field in the frame of the presented visual stimulus. The input-output mapping reflects retinal geometrical mapping between the targeted inner retinal cell's location on the retina and its corresponding visual field location. When the model cell produces a voltage output, such as an action potential, the corresponding group of mirrors are switched to the on-state to deliver light to drive optogenetic-expressing neurons.

When running the application, the system is clocked by the Vsync signal of the computer, which synchronizes the frame rate of graphics card and refresh rate of the DLP projector. During each frame period, a new frame of visual stimuli is generated, neural computation is performed by all the cell models to produce patterns of voltage signals (e.g., patterns of action potentials) in response to the visual stimuli, and the DLP projector displays spatially and temporally structured light pulses accordingly. In addition, an online safety monitor is implemented to keep track of the accumulative light exposure to ensure ocular safety.

III. METHODS AND PROCEDURES

In this section, we describe several key components of the application including stimuli generation, retinal geometrical mapping, neural computation, real-time processing, and light safety monitor.

A. STIMULI GENERATION

During each frame period, a frame of visual stimuli is generated, which corresponds to a square visual field of 25 degree on each side. The frame size is 500 × 500, and each pixel spans 0.05 degree of visual angle. The stimuli generator supports the following modes:

Flicker and visual field explore: In this mode, the system presents flash stimuli with adjustable duration, frequency, and field size. The module is designed to test the light pulse duration and intensity necessary to activate optogenetic proteins, and explore the visual field of optogenetically restored vision. All these are important for the design and customization of prosthetic devices.

Since the inner limiting membrane presents a physical barrier for the diffusion of viral vectors to the distal retina, the expression of transgene is typically limited to central retinal region [24]. To assess the extent of optogenetically restored vision, subjects can use a joystick to adjust the boundary of stimulating area: starting from an area large enough to cover the central retina, the user can decrease the size of light stimulation from one of the four directions (up, down, left, right), and monitor the size of the perceived light. When they feel it starts to shrink, they are approaching the boundary of the restored visual field from that direction. The user can repeat the above process to locate the boundaries from all other directions.

Grating: In this mode, the system presents square-wave gratings with adjustable spatial frequency, orientation, and speed. The grating stimuli can effectively assess the visual acuity of the subject.

Motion and direction: In this mode, the system presents a moving object (bar, circle, triangle, etc) with adjustable sizes, orientation, and speed. The mode is used to assess subject's ability to detect moving objects.

Object recognition: In this mode, the system presents pre-stored images of objects in everyday life (fruits and vegetables, household objects, letters, etc). The application offers flexibility to resize the image on the fly so that it can subtend different visual angles.

Live: In this mode, a frame of visual stimuli is captured from a camera in real-time, which allows subjects to detect and distinguish live actions, people, and objects in real world conditions. The application provides options to preprocess the frame with image processing techniques such as histogram equalization.

B. RETINAL GEOMETRICAL MAPPING

For optogenetic treatment, the light patterns used to stimulate an inner retinal cell is typically determined by the visual stimuli within its receptive field. However, it is nontrivial to find the receptive field location due to the inhomogeneous architecture of the central region of the primate retina, including humans. The central most area, the foveola (diameter about 300-400 μm or 1.1-1.4 degree), contains no inner retinal cells despite containing densely packed photoreceptors. This is to allow light to pass more easily through the tissue to reach the photoreceptors, which lie in the outermost layer of the retina (in the back of the eye). Each inner retinal cell is, therefore, displaced relative to the photoreceptors that create its receptive field. Below, we describe an efficient approach to address the challenge of retinal geometrical mapping. While ganglion cell is used as an example, the strategy is also applicable to other inner retinal cells (e.g., bipolar cells).

Based on specimens of vertical hemi-meridian of human subjects, a ganglion cell and its corresponding photoreceptor eccentricity can be described by the following equation [23]

$$e_c = \left(\frac{e_g}{1.29}\right)^{\frac{1}{0.67}} - 0.046 \tag{1}$$

where e_g is the ganglion eccentricity (mm) and e_c is corresponding cone eccentricity (mm). The relation holds up to an eccentricity of 2.254 mm; beyond this range, the displacement is assumed to 0, which means the location of ganglion cells and the corresponding cones are the same (i.e., $e_g = e_c$).

To account for uncertainties such as human variability, it is desirable to make the relation easily adjustable online. To meet this need, we come up with a class of functions parameterized by a morphing curvature w

$$e_c = b\left(\frac{e_g - a}{b - a}\right)^w \tag{2}$$

where $a = 0.164$ mm and $b = 2.254$ mm represent two boundary points. Specifically, a is the eccentricity of foveola. For $e_g < a$, there are no ganglion cells. For the ganglion cells at the boundary a, the corresponding cones are at the center of foveola (when $e_g = a$, $e_c = 0$). For the ganglion cells at the boundary b, the displacement becomes 0 (when $e_g = b$, $e_c = e_g$). The displacement only exists between a and b. As shown in Fig.2, the shape of the function can be adjusted by changing the curvature from linear ($w = 1$) to quadratic ($w = 2$). Especially, when $w = 1.37$, the function well approximates the results in (1) as shown in Fig.2. Note that, the same mapping (2) is assumed for all directions.

Given the relations above, the next step is to find the location of the receptive field center (the visual field center) of a target cell. In the application, both visual stimuli (given by input frames) and spatially distributed light stimulation (determined by output frames to the DLP) are in the form of an array of pixels. To establish the correspondence between input and output pixels, it is convenient to describe both in the same spatial coordinate system, in which each point is given a unique coordinate (x, y) in degrees of visual angle.

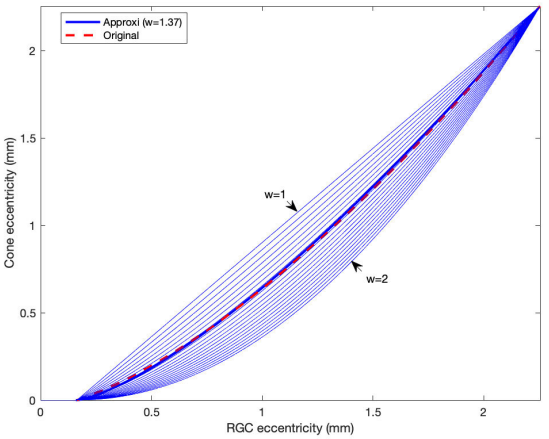

FIGURE 2. Geometrical mapping functions with an adjustable morphing curvature w. The x-axis represents the eccentricity of ganglion cells, and the y-axis represents the eccentricity of the corresponding cone photoreceptors. The shape of the function (2) changes from linear to quadratic as the morphing curvature w increases from 1 to 2. When $w = 1.37$, the function (2) well approximates the original relation (1) derived from specimens of human subjects.

Assume the coordinates of the array center are (0,0), the coordinates of all the pixels in both input and output frames can be calculated.

Assume the target is a ganglion cell at location (x_g, y_g), the location of the corresponding visual field center (x_c, y_c) is given by

$$x_c = x_g \cdot \frac{e_c}{e_g}, \quad y_c = y_g \cdot \frac{e_c}{e_g} \tag{3}$$

The receptive field is typically specified by a $P \times P$ array of pixels surrounding the center, and the coordinates of the P^2 pixels (x_{ci}, x_{cj}) can be calculated from the center as follows

$$x_{ci} = x_c - \left(\frac{P-1}{2} - i\right) \cdot L, \quad y_{cj} = y_c - \left(\frac{P-1}{2} - j\right) \cdot L \tag{4}$$

where L is the length of an input pixel, $i = 0, \ldots, P-1$, and $j = 0, \ldots, P-1$. Given the coordinates, we can take the values of the pixels at these locations as the inputs to the model cell at (x_g, y_g).

C. NEURAL COMPUTATION

In general, the conversion from visual stimuli to the light modulation needed for optogenetic stimulation is described by a mathematical model. Since the paper focuses on implementation aspects, a generic discrete-time firing rate model [30] is employed for the purpose of explication.

$$I_{(x_g,y_g)}[k] = -\sum_{q=1}^{Q} a_q I_{(x_g,y_g)}[k-q] + \sum_{i=0}^{P-1}\sum_{j=0}^{P-1}\sum_{m=0}^{M} b_{i,j,m} u_{(x_{ci},y_{cj})}[k-m] \tag{5}$$

where k is the integer-valued discrete-time index, the output $I_{(x_g,y_g)}$ represents the synaptic current entering the soma of neuron at location (x_g, y_g), $u_{(x_{ci},y_{cj})}$ is the input at location (x_{ci}, y_{cj}), and a_q and $b_{i,j,m}$ are constant coefficients. The equation shows a Qth order recursion process, i.e., the next value of the output is computed from the Q previous values of the output and the $P^2(M+1)$ values of the input. The inputs are obtained from pixels within the receptive field of the cell in the frames of visual stimuli, according to equations (2)(3)(4) as described in Section III-B.

Given $I_{(x_g,y_g)}[k]$, the firing rate of the neuron $\lambda_{(x_g,y_g)}[k]$ can be expressed as

$$\lambda_{(x_g,y_g)}[k] = F(I_{(x_g,y_g)}[k] + I_0) \tag{6}$$

where F is called an activation function, and I_0 is a constant offset which sets the baseline firing rate of the model.

Firing rate models can be used to generate stochastic spike sequences from a deterministically computed rate. A spike train is typically described by an inhomogeneous Poisson process, which involves a time-dependent firing rate $\lambda(t)$ [31]. If n is the observed number of spikes during a given time interval Δ, the probability of such an event is given by a Poisson distribution

$$P\left(n \mid \lambda\,(t)\right) = \frac{(\lambda(t)\Delta)^n}{n!}\exp(-\lambda(t)\Delta) \tag{7}$$

For sufficiently small intervals Δ, the probability of occurrence of more than one spike can be ignored, and the probability of a spike occurring is equal to the product of the instantaneous firing rate during that interval and the length of the interval

$$P(n = 1|\lambda(t)) = \lambda(t)\Delta \tag{8}$$

Given this, we divide the frame period T into J bins (each of width $\Delta = T/J$), perform a linear interpolation to calculate $I_{(x_g,y_g)}[k-1+j/J], j = 1, \ldots, J-1$, and calculate the firing rate at each bin as follows

$$\lambda_{(x_g,y_g)}[k]_j = F(I_{(x_g,y_g)}[k-1+j/J] + I_0) \tag{9}$$

To generate spikes, for the jth bin ($j = 1, \ldots, J$), we draw a Bernoulli random variable X with probability $\lambda_{(x_g,y_g)}[k]_j\Delta$. If $X = 1$, there is a spike; otherwise, there is no spike. Typically, the interval Δ are in the millisecond range, which is desired for the timing of neuronal spiking.

D. REAL-TIME PROCESSING

When running the application, the light stimulator receives frames from the computer over a HDMI connection. During each frame period, the stimuli generator produces a new frame of visual stimuli, neural computations are performed on all the cell models to produce sequences of spikes, and the DLP stimulator delivers spatially and temporally structured light pulses accordingly. As all these operations need to be completed within a frame period, a real-time constraint is imposed on the application.

For each model cell, the inputs are determined by pixels within its receptive field, which can be determined by retinal geometrical mapping as described in Section III-B, and the spikes are generated from the results of neural computation as described in Section III-C. Specifically, we choose $J = 24$ in Equation (9), and thus divides the frame period into 24 bins. The spike train of the model cell is stored with a 24-bit binary number, where a 1 at the ith bit indicates a spike in the ith bin ($i = 0, \ldots, 23$). To direct the DLP to deliver patterns of light accordingly, the binary number is written into the corresponding output pixels of the cell in a framebuffer as 24-bit RGB values: bits 0-7 are written into bits 0-7 of byte Blue, bits 8-15 are written into bits 0-7 of byte Red, and bits 16-23 are written into bits 0-7 of byte Green. In the implementation, the mapping of input and output pixels onto each model cell are stored in a lookup table, which can be quickly consulted in the real-time simulation.

All the above procedures need to be finished before the arrival of the next refresh signal (Vsync) to meet the real-time constraints. Upon the arrival of Vsync, the 24-bit RGB frame is sent to DLP, which decomposes it into 24 binary patterns and display the patterns in sequence for optogenetic stimulation. In the meanwhile, the program returns to the beginning of the loop to generate a new frame of visual stimuli.

Note that the program allows users to adjust a variety of features in real time such as retinal geometrical mapping, optogenetic stimulating range and location, and properties of the visual stimuli (e.g, size, shape, orientation, speed, etc), via a graphic user interface (GUI) or a joystick. The program updates these parameters at the beginning of every frame period so that the changes could take effect immediately.

E. LIGHT SAFETY MONITOR

Light safety has been a concern for clinical applications of optogenetics, as early channelrhodopsins required bright light of relatively short wavelengths [1]. However, this problem has been significantly reduced by later developed optogenetic proteins due to higher light sensitivity or longer activation wavelength [25]. However, studies by Morgan et al. [26], [27] in non-human primates showed retinal damage was occurring from exposures to 568 nm light at intensity levels below those reported in ANSI 2007. To account for these studies, a new limit termed Luminance Dose Restriction has been added to the 2014 ANSI [28] (Section 8.3) as an interim precaution.

Briefly, for exposures that occur within a 48 hour window and exceed 100 seconds, the cumulative retinal radiant exposure should be below $5/V(\lambda)$, where $V(\lambda)$ is the photopic luminous efficiency function and the units for $5/V(\lambda)$ are in J/cm^2. As shown in Fig.3 (top), the photopic luminous efficiency function peaks at 555 nm and decreases toward both ends of the spectrum.

The luminance dose restriction is worth attention as it lowers the safety margin of optogenetic proteins with longer activation wavelength, which were previously supposed to be sufficiently safe. For example, Fig.3 (bottom) shows the

IEEE Journal of Translational Engineering in Health and Medicine

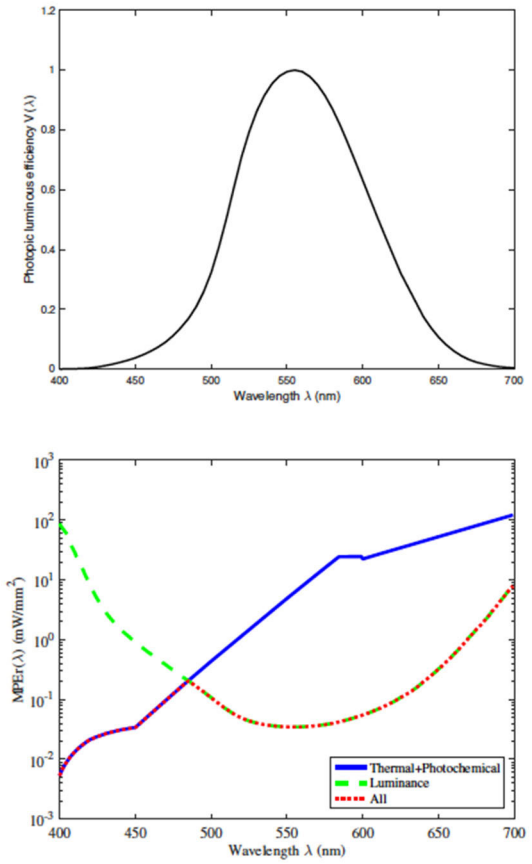

FIGURE 3. Luminance dose restriction. Top: photopic luminous efficiency function. Bottom: the maximum permissible retinal irradiance for light stimulation (5msec pulse width, 10 Hz frequency, 8 hours) as a function of wavelength. The limits are calculated based on the computer implementation of 2014 ANSI for optogenetic stimulation [32].

maximum permissible retinal irradiance for light stimulation (5 msec pulse width, 10 Hz frequency, 8 hours) as a function of wavelength, where blue line shows the conventional thermal and photochemical limit, which largely increases as wavelength increases. The green dashed line shows the limit of luminance dose restriction, which is the strictest at 555 nm. We can see the final limit (red dotted line, obtained by taking a minimum of the two) is lowered than the conventional limit (blue line) for longer wavelengths.

In view of this, we implement an online light safety monitoring module based on the luminance dose restriction in our application. Briefly, we keep track of the accumulative retinal exposure at each output pixel, and make sure the maximum exposure among all pixels is less than a threshold. If the threshold is reached, the light delivery will be stopped by the application.

As the light pattern is composed of identical pulses, it boils down to counting the total number of pulses at each pixel so that

$$max_k(N_k) \cdot \tau \cdot E_r \leq f \frac{5}{V(\lambda)} \tag{10}$$

where N_k is the number of light pulses at the kth pixel, τ is the light pulse duration, E_r is the retinal irradiance, and a factor f ($f < 1$) is set to be more conservative.

When running the application, the maximum accumulative exposure among all pixels is saved to a log file in real time. This allows the record to be kept when the application is exited. The data in log file is loaded when the application is relaunched to ensure continuous monitoring throughout the time.

IV. RESULTS

In this section, we demonstrate the design and performance of the application for optogenetic gene therapy of retinal degenerative diseases.

A. SYSTEM SPECIFICATION

Fig.4 (left) shows the light stimulator, which targets a square visual field of 24 degree on each side. The field of view is large enough to cover the macula (a round area of 18 degree in diameter at the center of retina), which is sufficient as the expression of optogenetic gene is typically restricted to central para-foveal area (less than 10 degree in diameter at the center of macula) due to inner limiting membrane barriers [24]. The retinal image size of each micromirror is 0.05 degree (14 μm), which determines the maximal spatial resolution. From software point of view, a lower spatial resolution can be achieved by using a $s \times s$ ($s > 1$) pixel group as a super-pixel, and thus the size of each super-pixel determines the spatial resolution of light stimulation.

The system allows to choose one of the three LEDs (blue: 460nm, green: 515nm, red: 617nm). The maximal retinal irradiance is 1.4mW/mm^2, 1.1mW/mm^2, and 1.2mW/mm^2, respectively, which are sufficient to activate most optogenetic proteins of clinical interests [25]. For example, a new channelrhodopsin with fast kinetics and high light sensitivity, Chronos (peak activation wavelength: 500nm), reliably drove 100% spiking at light powers as low as 0.05mW/mm^2 [25]. The light levels can be reduced by adding neutral density filters or decreasing the current through the LEDs.

The light stimulator is controlled by a software application developed using C++. Fig.4 (right) shows the graphic user interface (GUI) of the software in the training mode, which allows users to set and adjust parameters for various functional modules to control stimulating range and resolution, visual stimuli generation and presentation, retinal geometrical mapping, light safety monitoring, and so forth. Below, we use examples to demonstrate the functions of key modules.

B. VISUAL STIMULI GENERATION

Fig.5 shows examples of visual stimuli presented by the software including a moving bar, drifting square-wave gratings, a letter A, and an object banana. The moving bar and gratings are generated online with adjustable parameters such as spatial frequency, orientation, and moving speed: the bar

FIGURE 4. Light stimulator and software application. Left: the light stimulator with a chin rest and a button box. When looking through the eyepiece, the light is delivered to activate light-sensitive proteins in retinal cells. Neutral density filters can be inserted to adjust the light levels. Right: the graphic user interface (GUI) of the software in the training mode, which allows users to set and adjust parameters for various functional modules to control stimulating range and resolution, visual stimuli generation and presentation, retinal geometrical mapping, light safety monitoring, and so forth.

is 1 degree wide and 8 degree high, moving to the right at a speed of 4.25 deg/sec; the grating has a temporal frequency of 1 Hz and a spatial frequency of 0.2 cpd (the spatial period of the grating is 5 degree), drifting to the right at a speed of 5 deg/sec. The letter and banana are generated from pre-stored images and the sizes can be adjusted by users online.

C. RETINAL GEOMETRICAL MAPPING

To generate neural responses to these visual stimuli, one important aspect is retinal geometrical mapping due to the displacement between the locations of inner retinal cells and the corresponding cones. For ganglion cells, the relation is described by a function (2) with an easily adjustable morphing curvature w as shown in Fig. 2. The software allows to adjust the curvature continually online by a researcher/clinician using the GUI, or by a subject using a joystick. In this way, subjects can find the curvature that works the best as a starting point for further optimization. This is similar to the case of a refraction test: an optometrist cycles through different lenses to find the one that help the subject see best.

Given a geometric mapping, neural computation is carried out in real-time. To demonstrate the effects of different morphing curvatures, stimuli at the receptive field center of all the model cells are shown in Fig.6 (i.e., what each individual cell sees at its own location during one frame period). Note that there is a dark circular spot (about 1 degree in diameter) at

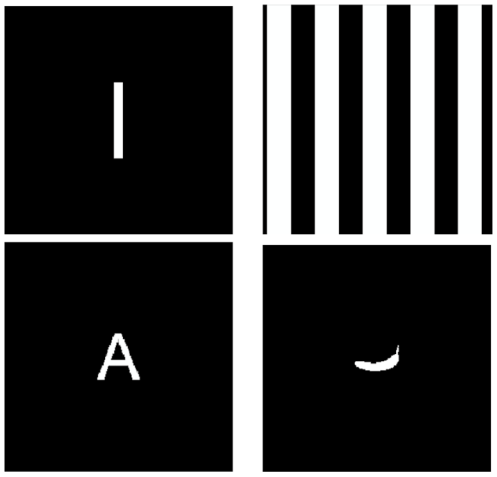

FIGURE 5. Visual stimuli presented by the software. Top left: a vertical moving bar (width: 1 degree, height: 8 degree) moving to the right at a speed of 4.25 deg/sec; Top right: square-wave gratings (spatial period: 5 degree), drifting to the right at a speed of 5 deg/sec; Bottom left: letter A (height: 5 degree); Bottom right: object banana (width: 5 degree). Each panel corresponds to a square field of view of 25 degree on each side. The users can see the stimuli from the GUI (Fig. 4) when running the software and can get immediate feedback when making online adjustment.

the center of each panel. This spot corresponds to foveola, the central most area in the human fovea, which contains no inner retinal cells. The cones in foveola are connected to ganglion cells centrifugally displaced in the surrounding region. In the first row of Fig.6, as the 1 degree wide bar passes foveola,

IEEE Journal of Translational Engineering in Health and Medicine

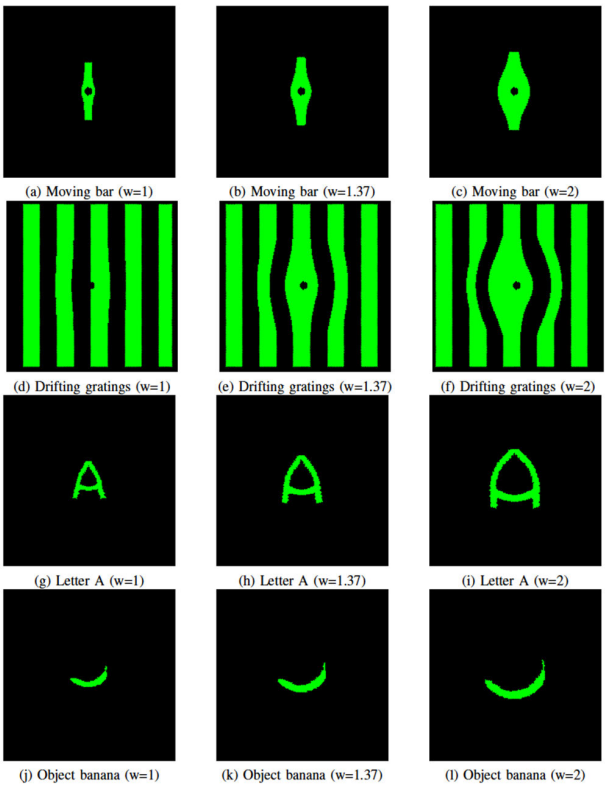

FIGURE 6. **The visual stimuli at the receptive field center of all the model cells (i.e., what each individual cell sees at its own location during one frame period) with different morphing curvatures (Fig. 2). The original stimuli are shown in Fig. 5. Each panel corresponds to a square field of view of 24 degree on each side. The total number of model cells is 23545 and the spatial resolution is 0.15 degree.**

there is a distortion of the shape: the middle segment of the bar deforms into a ring surrounding foveola. As the morphing curvature w increases from 1 to 2, the displacement between cones and ganglion cells increases, leading to an expansion of the ring size. The bar stimuli can be used to test if the morphing curvature matches the subject's own retinal architecture. If so, the subject would perceive a straight bar even though the distorted version is presented for optogenetic stimulation of ganglion cells.

The displacement between ganglion cells and corresponding cones remains up to an eccentricity of 7.8 degree. This is evident in the case of grating stimuli (Fig.6f): only the bars in the central region are deformed, which roughly covers three spatial cycles of gratings (each cycle spans 5 degree). Beyond this range, the bars remain straight.

In general, the effects of deformation are dependent on the shape of the object and its location relative to the center of the field. As shown in the third row of Fig.6, the letter A becomes less recognizable as the morphing curvature increases. In contrast, the banana (the last row of Fig.6) still looks like a banana in all cases despite a change of size. This is because the banana is a curved shape towards foveola. Overall, the shape of a circular object centered at foveola is less subject to deformation.

TABLE 1. **The number of model cells that can be processed in real-time and the corresponding spatial range (in parentheses) under different conditions of temporal and spatial resolutions. The spatial range is given by the size length of a square visual field.**

Spatial resolution \ Temporal resolution	0.7 msec (1440Hz)	1.4 msec (720Hz)	2.8 msec (360Hz)
0.05°	19.4K (7.3°)	68.8K (13.7°)	171.1K (21.6°)
0.10°	19.0K (14.5°)	*	*
0.15°	17.9K (21.1°)	*	*

*The number of cells that can be processed in real-time is more than the number of cells required to fill the whole field (i.e., a square visual field of 24 degree on each side).

D. REAL-TIME PERFORMANCE AND SCALABILITY

From a practical point of view, it is desirable that the application can be run in real-time on a regular computer in clinical settings. Toward this direction, we assess the scalability under real-time constraint, which is measured by the number of model cells described by (5) and (9) with ($Q = 1$, $M = 9$, $P = 3$, $J = 24$) that can be processed in real-time on a desktop (CPU: Intel Core i7-10700K 3.8 up to 5.1 GHz, memory: 32 GB). Note that it takes a total cost of $O(Q+P^2(M+1)+cJ)$ to simulate the model cell during each frame period [30]. The results under different conditions of temporal and spatial resolutions are given in Table 1.

The temporal resolution is determined by the pattern rate of the DLP in the monochrome mode (1440Hz, 720Hz, 360Hz), which equals 24 times the frame rate (60Hz, 30Hz, 15Hz) being used. Given a longer frame period, the temporal resolution is lower but more model cells can be processed during the frame period. So there is a tradeoff between temporal resolution and scalability. As shown in the second row of the Table 1, given a spatial resolution of 0.05 degree, the number of model cells that can be processed in real-time under temporal resolutions of 1440Hz, 720Hz, and 360Hz is 19.4K, 68.8K, and 171.1K, respectively. The spatial resolution is given by the size of super-pixels.

As shown in the second column, given a temporal resolution of 1440Hz, the stimulating area under spatial resolution of 0.05°, 0.10°, and 0.15° is 7.3°, 14.5°, and 21.1°, respectively, which means a lower resolution makes it possible to stimulate a larger area given limited computing power. In addition, as the spatial range of optogenetic stimulation increases, the number of model cells decreases slightly. This is because a larger stimulating area requires a larger visual field (and thus a larger image) to be processed during each frame period.

Overall, under real-time constraints, the application satisfies key requirements for optogenetic retinal stimulation: it provides millisecond resolution desired for precise control of neuronal spiking [33]; the stimulating range is sufficient to cover the transgene expression, which is typically limited to the central para-foveal ring of retina (<10°) [24]; the spatial

resolution can reach up to 0.05° (14μm on retina), which is comparable to the size of ganglion cells in the central retina [34].

V. DISCUSSION

In this paper, we present an engineering platform for clinical application of optogenetic therapy for retinal degenerative diseases. In the treatment, the remaining retinal cells are rendered photosensitive by expressing light-sensitive proteins [6], [7], [8], [9], [10], [11], [12], [13], [14], [20], which typically require bright light at specific wavelengths for effective activation, and additional processing units to convert visual stimuli to the spatial and temporal patterns of the light stimulation to reflect visual processing of the bypassed retinal circuitry. These make the assessment of the treatment more challenging than conventional gene therapies aiming to rescue photoreceptors [35], where existing ophthalmic equipment and vision testing procedures are readily available.

In light of this, it is highly desirable to have a clinical platform so that researchers and clinicians can assess and explore the vision of subjects in optogenetic therapy. Taking the first step towards this direction, we developed a hardware and software platform for clinical training, testing, and rehabilitation. The system consists of a DLP-based light stimulator, capable of delivering light with sufficient intensity as well as spatial and temporal resolution, and a software application, which converts visual stimuli into light patterns in real time to mimic neural processing. Note that the system can be integrated with a commercial fundus-controlled perimetry device (i.e., microperimetry) to achieve retinal tracking while performing light stimulation as demonstrated in an earlier work [36]. This allows precise control of stimulation sites, which is valuable for subjects who have difficulty controlling their eye movements.

The platform can be used not only to measure the outcome of clinical studies but also provide guidance for the design and prescription of prosthetic devices to maximally utilize the optogenetically-restored vision. For optogenetic treatment, the design of prosthetic devices has a direct impact on the restored vision. The prosthetic device is typically in the form of a pair of goggles allowing for mobility in real world settings, which includes a camera, a microcontroller, and a DLP-based near eye display. The conversion from camera stimuli to light stimulation is governed by a variety of parameters such as intensity and duration of light pulses, spatial and temporal resolution, geometrical mapping, and the neural model being used. To make the device suitable for a particular subject, these parameters that need to be optimized, which requires a trial-and-error method, similar to the case of a refraction test (i.e., an optometrist cycles through different lenses to find the one that help the subject see best), but much more complicated. The platform has provided the capability to make this process systematic, efficient and tractable.

In addition, the platform can also be used for the purpose of rehabilitation. Since the optogenetically-restored vision is likely to be different from natural vision in some aspects (depending on the neural model used), the brain may need to learn to interpret and harness the perceived information. To speed up this process, it is helpful for subjects to undergo supervised rehabilitation with clinicians to sharpen the re-established neural circuitry, regain the control of eye movements, re-learn eye/hand coordination, and explore ways to maximally utilize the newly restored vision offered by the treatment, especially for people who have been visually impaired for a long time. The platform has provided a tool for clinical rehabilitation to achieve these goals.

More generally, the applicability is not limited to optogenetic therapy. For example, methods based on chemical photoswitches have been developed in recent years (as reviewed in [22]), where chemically synthesized photosensitive molecules are employed for manipulating the activation of inner retinal cells, which also require bright light at specific wavelengths. In addition, the expression of genetically modified receptors (which can attach the photosensitive molecules) in inner retinal cells are also achieved via AAV-mediated delivery [37]. As a result, these methods share many similar needs and challenges with optogenetic approaches, making the platform applicable in the upcoming clinical stage.

VI. CONCLUSION

In this translational study, we have developed an engineering platform for clinical application of optogenetic therapy for retinal degenerative diseases, to measure the outcome of clinical studies and provide guidance for the design and prescription of prosthetic devices. The platform consists of a DLP-based stimulator, capable of delivering light with sufficient intensity as well as spatial and temporal resolution, and a software application, which drives the light stimulator to conduct clinical training, testing, and rehabilitation for optogenetic gene therapy. Key components of the application include stimuli generation, retinal geometrical mapping, real-time neural computation, and light safety monitoring. Examples are given to demonstrate the functionality and scalability of the application in real time processing. The results show the platform meets the requirements for optogenetic retinal stimulation.

ACKNOWLEDGMENT

Boyuan Yan is a Consultant with Bionic Sight Inc. Sheila Nirenberg is the Principal and the Founder of Bionic Sight Inc.

REFERENCES

[1] G. Nagel et al., "Channelrhodopsin-2, a directly light-gated cation-selective membrane channel," *Proc. Nat. Acad. Sci. USA*, vol. 100, no. 24, pp. 13940–13945, Nov. 2003.

[2] F. Zhang et al., "Multimodal fast optical interrogation of neural circuitry," *Nature*, vol. 446, no. 7136, pp. 633–639, 2007.

[3] X. Han et al., "Millisecond-timescale optical control of neural dynamics in the nonhuman primate brain," *Neuron*, vol. 62, no. 2, pp. 191–198, 2009.

[4] L. Petreanu, D. Huber, A. Sobczyk, and K. Svoboda, "Channelrhodopsin-2–assisted circuit mapping of long-range callosal projections," *Nature Neurosci.*, vol. 10, no. 5, pp. 663–668, 2007.

[5] O. G. S. Ayling, T. C. Harrison, J. D. Boyd, A. Goroshkov, and T. H. Murphy, "Automated light-based mapping of motor cortex by photoactivation of channelrhodopsin-2 transgenic mice," *Nature Methods*, vol. 6, no. 3, pp. 219–224, Mar. 2009.

[6] A. Bi et al., "Ectopic expression of a microbial-type rhodopsin restores visual responses in mice with photoreceptor degeneration," *Neuron*, vol. 50, pp. 23–33, Apr. 2006.

[7] P. S. Lagali et al., "Light-activated channels targeted to ON bipolar cells restore visual function in retinal degeneration," *Nature Neurosci.*, vol. 11, no. 6, pp. 667–675, Jun. 2008.

[8] H. Tomita et al., "Channelrhodopsin-2 gene transduced into retinal ganglion cells restores functional vision in genetically blind rats," *Exp. Eye Res.*, vol. 90, no. 3, pp. 429–436, Mar. 2010.

[9] M. M. Doroudchi et al., "Virally delivered channelrhodopsin-2 safely and effectively restores visual function in multiple mouse models of blindness," *Mol. Therapy*, vol. 19, no. 7, pp. 1220–1229, Jul. 2011.

[10] S. Nirenberg and C. Pandarinath, "Retinal prosthetic strategy with the capacity to restore normal vision," *Proc. Nat. Acad. Sci. USA*, vol. 109, no. 37, pp. 15012–15017, Sep. 2012.

[11] E. Macé et al., "Targeting channelrhodopsin-2 to ON-bipolar cells with vitreally administered AAV restores ON and OFF visual responses in blind mice," *Mol. Therapy*, vol. 23, no. 1, pp. 7–16, Jan. 2015.

[12] A. Chaffiol et al., "A new promoter allows optogenetic vision restoration with enhanced sensitivity in macaque retina," *Mol. Therapy*, vol. 25, no. 11, pp. 2546–2560, 2017.

[13] S. Batabyal, S. Gajjeraman, S. Pradhan, S. Bhattacharya, W. Wright, and S. Mohanty, "Sensitization of ON-bipolar cells with ambient light activatable multi-characteristic opsin rescues vision in mice," *Gene Therapy*, vol. 28, nos. 3–4, pp. 162–176, Apr. 2021.

[14] G. Gauvain et al., "Optogenetic therapy: High spatiotemporal resolution and pattern discrimination compatible with vision restoration in non-human primates," *Commun. Biol.*, vol. 4, no. 1, pp. 1–15, Jan. 2021.

[15] AbbVie. *RST-001 Phase I/II Trial for Advanced Retinitis Pigmentosa*. Accessed: Oct. 1, 2023. [Online]. Available: https://clinicaltrials.gov/ct2/show/NCT02556736

[16] GenSight Biologics. *Dose-Escalation Study to Evaluate the Safety and Tolerability of GS030 in Subjects With Retinitis Pigmentosa*. Accessed: Oct. 1, 2023. [Online]. Available: https://clinicaltrials.gov/ct2/show/NCT03326336

[17] Bionic Sight. *BS01 in Patients With Retinitis Pigmentosa*. Accessed: Oct. 1, 2023. [Online]. Available: https://clinicaltrials.gov/ct2/show/NCT04278131

[18] Nanoscope Therapeutics. *Efficacy and Safety of vMCO-010 Optogenetic Therapy in Adults With Retinitis Pigmentosa*. Accessed: Oct. 1, 2023. [Online]. Available: https://clinicaltrials.gov/ct2/show/NCT04945772

[19] S. Nirenberg, "Positive interim results in bionic sight's optogenetic gene therapy trial," presented at the 2nd Annu. Gene Therapy Ophthalmic Disorders, 2021.

[20] J.-A. Sahel et al., "Partial recovery of visual function in a blind patient after optogenetic therapy," *Nature Med.*, vol. 27, no. 7, pp. 1223–1229, Jul. 2021.

[21] S. Mohanty, "Exploring ambient light activatable optogenetics for vision restoration in retinal degenerative diseases," presented at the 3rd Annu. Gene Therapy Ophthalmic Disorders, 2022.

[22] I. Tochitsky, M. A. Kienzler, E. Isacoff, and R. H. Kramer, "Restoring vision to the blind with chemical photoswitches," *Chem. Rev.*, vol. 118, no. 21, pp. 10748–10773, Nov. 2018.

[23] J. Sjöstrand, Z. Popovic, N. Conradi, and J. Marshall, "Morphometric study of the displacement of retinal ganglion cells subserving cones within the human fovea," *Graefe's Arch. Clin. Exp. Ophthalmol.*, vol. 237, no. 12, pp. 1014–1023, Nov. 1999.

[24] M. E. McClements, F. Staurenghi, R. E. MacLaren, and J. Cehajic-Kapetanovic, "Optogenetic gene therapy for the degenerate retina: Recent advances," *Frontiers Neurosci.*, vol. 14, pp. 1–17, Nov. 2020.

[25] N. C. Klapoetke et al., "Independent optical excitation of distinct neural populations," *Nature Methods*, vol. 11, no. 3, pp. 338–346, Mar. 2014.

[26] J. I. Morgan et al., "Light-induced retinal changes observed with high-resolution autofluorescence imaging of the retinal pigment epithelium," *Invest. Ophthalmol. Vis. Sci.*, vol. 49, no. 8, pp. 3715–3729, 2008.

[27] J. I. Morgan, J. J. Hunter, W. H. Merigan, and D. R. Willams, "The reduction of retinal autofluorescence caused by light exposure," *Invest. Ophthalmol. Vis. Sci.*, vol. 50, no. 12, pp. 6015–6022, 2009.

[28] *American National Standard for Safe Use of Lasers*, Standard ANSI 136.1-2014, ANSI, The Laser Institute of America, 2014.

[29] D. Dudley, W. M. Duncan, and J. Slaughter, "Emerging digital micromirror device (DMD) applications," *Proc. SPIE*, vol. 4985, pp. 1–12, Jan. 2003.

[30] B. Yan and S. Nirenberg, "An embedded real-time processing platform for optogenetic neuroprosthetic applications," *IEEE Trans. Neural Syst. Rehabil. Eng.*, vol. 26, no. 1, pp. 233–243, Jan. 2018.

[31] P. Dayan and L. F. Abbott, *Theoretical Neuroscience: Computational and Mathematical Modeling of Neural System*. Cambridge, MA, USA: MIT Press, 2001.

[32] B. Yan, M. Vakulenko, S. H. Min, W. W. Hauswirth, and S. Nirenberg, "Maintaining ocular safety with light exposure, focusing on devices for optogenetic stimulation," *Vis. Res.*, vol. 121, pp. 57–71, Apr. 2016.

[33] E. S. Boyden, F. Zhang, E. Bamberg, G. Nagel, and K. Deisseroth, "Millisecond-timescale, genetically targeted optical control of neural activity," *Nature Neurosci.*, vol. 8, no. 9, pp. 1263–1268, Sep. 2005.

[34] R. Hebel and H. Holländer, "Size and distribution of ganglion cells in the human retina," *Anatomy Embryol.*, vol. 168, no. 1, pp. 125–136, Oct. 1983.

[35] A. M. Maguire, J. Bennett, E. M. Aleman, B. P. Leroy, and T. S. Aleman, "Clinical perspective: Treating RPE65-associated retinal dystrophy," *Mol. Therapy*, vol. 29, no. 2, pp. 442–463, Feb. 2021.

[36] A. V. Cideciyan et al., "Developing an outcome measure with high luminance for optogenetics treatment of severe retinal degenerations and for gene therapy of cone diseases," *Invest. Ophthalmol. Vis. Sci.*, vol. 57, no. 7, pp. 3211–3221, 2016.

[37] B. M. Gaub et al., "Restoration of visual function by expression of a light-gated mammalian ion channel in retinal ganglion cells or ON-bipolar cells," *Proc. Nat. Acad. Sci. USA*, vol. 111, no. 51, pp. E5574–E5583, Dec. 2014.